Preprint Cambridge Centre for Computational Chemical Engineering ISSN 1473 – 4273

Lifting a buried object: reverse hopper theory

Kok Foong Lee, John F. Davidson, Jethro Akroyd, Markus Kraft [1]

released: 28 June 2013

[1] Department of Chemical Engineering
and Biotechnology
University of Cambridge
New Museums Site
Pembroke Street
Cambridge, CB2 3RA
United Kingdom
E-mail: mk306@cam.ac.uk

Preprint No. 129

Keywords: mathematical modelling, fluidisation, granular materials, particle, buried object, lifting

Edited by
Computational Modelling Group
Department of Chemical Engineering and Biotechnology
University of Cambridge
New Museums Site
Pembroke Street
Cambridge CB2 3RA
United Kingdom

Fax: + 44 (0)1223 334796
E-Mail: c4e@cam.ac.uk
World Wide Web: http://como.cheng.cam.ac.uk/

Abstract

A theory is given to predict the upward force, F, to lift an object buried at depth H in granular material. The object is either (1) a horizontal disc of diameter D or (2) a horizontal plate of width B and length L, where $L \gg B$. In case (1), the lifted disc is assumed to cause axi-symmetric upward particle motion, *reverse hopper flow*, within an inverted cone. *Active* failure is assumed: the vertical stress, σ_2, is $K \times$ (horizontal stress σ_1); here $K = (1+\sin\phi)/(1-\sin\phi)$, ϕ being the angle of friction for the granular material. This gives the vertical stress, σ_{20}, on the disc. An additional lift force is needed to overcome the frictional stress, τ, at the conical interface between stationary and upward moving particles: it is assumed that $\tau = \mu\sigma_1$, μ being the internal friction coefficient. For consolidated granules, $\mu = \tan\phi$, but for the sheared material, $\mu < \tan\phi$. The total lift force F is the sum of (i) the effect of σ_{20} plus (ii) the effect of τ; this sum gives an equation to predict the *breakout factor* $N_{\rm qf} = F/(\gamma' AH)$, where $\gamma' =$ bulk weight density and $A = \pi D^2/4$. For case (2), relevant to the uplift of a long buried pipe, the theory is similar: the two failure surfaces are flat, inclined at angles $+\alpha$ and $-\alpha$ to the vertical. Similar assumptions as to the stress distribution, i.e. two-dimensional *active* failure, give an equation for $N_{\rm qf}$. The two predictive equations for cases (1) and (2) agree well with relevant published measurements of $N_{\rm qf}$.

Contents

1 Introduction

This work began with a study of gas distributors for industrial fluidised beds. Such distributors often consist of a flat horizontal plate containing a number of nozzles through which gas flows to fluidise the particles above. The nozzles are separated by a horizontal distance, typically 10 - 20 cm; thus the bed of particles is fluidised by upward facing gas jets emerging from nozzles which may be a few centimetres diameter, separated by the horizontal distance 10 - 20 cm mentioned above.

Particles within each nozzle need only a modest gas flow for fluidisation, far less than the flow required to fluidise the main particle bed supported on the distributor. The question then arises: '*At what gas velocity through each nozzle will the whole bed be fully fluidised and what is the behaviour of the particles immediately above each nozzle*?' To fluidise the whole bed, a superficial velocity U_{mf} is needed, when the velocity in each nozzle will be $A_{\mathrm{b}}U_{\mathrm{mf}}/a$ where A_{b} is the bed area and a is the total area of the nozzles. Particles in the nozzles will be more than fully fluidised, because A_{b}/a is large. This paper deals with the situation where the nozzle gas velocity, U_{N}, is intermediate, i.e. $U_{\mathrm{mf}} < U_{\mathrm{N}} < A_{\mathrm{b}}U_{\mathrm{mf}}/a$. Thus each nozzle is fully fluidised but the main bed is not. In this situation, the particles above the nozzle will be subjected to forces of two kinds namely:

i) pressure gradients in the gas due to the outflow of gas from each nozzle into the main bed, and

ii) interparticle forces arising from the particles near the nozzle having an interstitial gas flow in excess of U_{mf}: this gas flow pushes the particles upwards so that they can press on the particles above, resulting in interparticle stresses.

This paper is concerned with these interparticle stresses and attempts to answer the question: '*What is the level of interparticle stress needed to push up the particles above*?' This question is similar to the question posed by workers in soil mechanics: '*If an object is buried in granular material, what upward force is needed to lift it*?' The answer to the latter question is given here by using well-established theory of hopper flow, but in reverse, i.e. upward rather than downward particle motion. In hopper theory ([10], [27]) granular material flows out of a hopper, as in an hour glass. The theory, based on the assumption of frictionless hopper walls, gives values which agree with experimental data, e.g. that the flow rate is proportional to (outlet diameter)$^{5/2}$. For hopper flow, the granular material is in the *passive state*, i.e. (horizontal stress) $= K \times$ (vertical stress), where $K = (1+\sin\phi)/(1-\sin\phi)$, $\tan\phi$ being the internal friction coefficient of the granular material.

In reverse hopper flow, the pushed up material is assumed to be in the *active state*, i.e. (vertical stress) $= K \times$ (horizontal stress). There is the further assumption that the displaced material moves within a cone whose axis is vertical. With these assumptions, the force at the bottom of the cone can be calculated. This force due to the normal stresses is less than the observed force. This appears to be because the conical interface between the upward moving and stationary material is assumed to be smooth. When a frictional force is allowed for, the total uplift force appears to be in good agreement with a wide range of experimental results.

The **purpose of this paper** is to present the newly developed reverse hopper theory for predicting the uplift force against a surcharge of granular material. Two versions of the theory are given:

i) *Axi-symmetric*: Here the pushed up granular material is assumed to be of conical form, i.e. the motion is axi-symmetric.

ii) *Two-dimensional*: Here the boundaries between upward moving granules and stationary granular material are assumed to be two flat interfaces symmetrically aligned about the central vertical axis, forming a two-dimensional flow pattern.

2 Literature review

The published research into fluidisation is primarily focused on predicting the hydrodynamics of fluidised systems with relatively few published works related to the start-up of industrial fluidised beds. Besides the well known group classification of Geldart [14], which enables the prediction of some fluidisation properties in terms of particle size and density, the minimum fluidising velocity and the bed expansion characteristics (as a function of bed porosity) are the two most widely studied design parameters for fluidised beds. Di Felice [11] presented a comprehensive review on the theoretical development regarding the hydrodynamics of liquid fluidisation.

A similar problem to that investigated in this work is the uplift of anchors and pipes, studied in geotechnical engineering. The following section reviews the relevant research in geotechnical engineering.

2.1 Insights from geotechnical problems

There are two main types of uplift problem in geotechnical engineering. The first category is related to the upheaval buckling of offshore pipelines buried in the seabed. These pipelines transport high-temperature oil and undergo upheaval buckling as a result of thermal expansion [16]. This phenomenon is one of the key failure modes of such pipelines and has serious economic and environmental consequences [8].

The second category is related to the study of plate anchors buried in sand. These plates are used in foundation systems where they are fixed to a building structure and embedded in the ground at sufficient depth to resist pullout forces [21].

For both applications, the uplift force is important. Thus the main design challenge for buried plates or pipelines is to determine the minimum depth of soil cover that will provide sufficient uplift resistance. The uplift resistance provided by the soil cover increases with depth, but the cost of the burial increases with depth and constitutes a significant fraction of the total construction cost. Therefore, burial depth should be minimised while providing sufficient uplift resistance [8]. This is the motivation behind most of the work in geotechnical engineering.

Currently, there are two main approaches to model the uplift of anchors and pipes in soils. The first approach uses variations of the Vertical Slip Model of Matyas and Davis [19]. This is often referred to as the limit equilibrium method. This assumes that the uplift force is the sum of the weight of the soil being lifted and the shear force along the failure surface. Recently, White et al. [31] presented a limit equilibrium solution for the vertical pullout of pipes and plate anchors buried in sand. The authors included the stress-dilatancy correlations presented by Bolton [6] in their equilibrium solution. The second approach is the finite element method, successfully applied by Merifield and Sloan [21] to predict the deformation mechanism during anchor uplift.

The uplift experiments reported in the literature were mostly carried out in a laboratory scale tank containing sand. The plates or pipes were embedded in the sand at a specified depth and connected, via a rod, to a load cell fixed above the tank. They were displaced at a constant pull-out rate using a gearbox. The displacement and uplift force were continuously monitored and recorded using displacement transducers and load cells.

A three-phase behaviour, illustrated in **Figure 1**, is usually observed in uplift tests reported in the literature ([8], [15], [22], [26]).

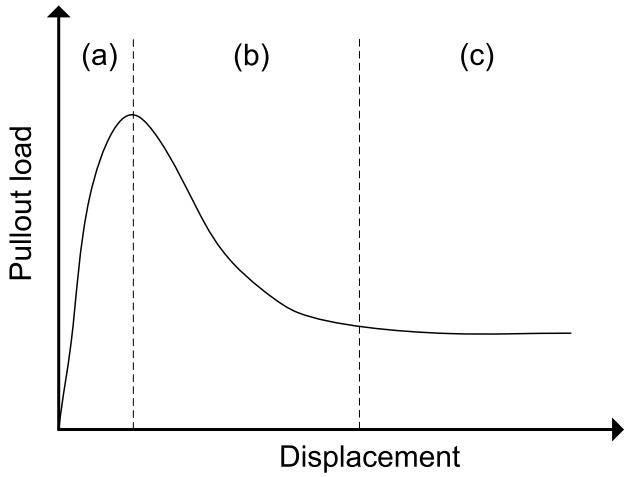

Figure 1: *Typical relationship between pullout load and displacement for uplift of plates/pipes in sand, with three different phases indicated in the figure.*

Referring to Figure 1, the first phase is the pre-peak behaviour, exhibiting a rapid increase in load. The second phase is the post-peak behaviour; the load decreases rapidly as displacement increases. The third phase is the residual behaviour, associated with a gradual decrease in load at large displacements [15].

Cheuk et al. [8] presented a detailed analysis on the three-phase behaviour illustrated in Figure 1. **Figure 2** summarises the results of Cheuk et al. [8] on the deformation mechanism during pipe uplift using PIV (particle image velocimetry). Figure 2(a) shows the formation of a trapezoidal sliding block at peak force. Figure 2(b) depicts the second phase, associated with infilling of soil into the gap formed below the pipe during uplift. After the infilling stage, a flow-around mechanism, Figure 2(c), is accompanied by a reduction in uplift resistance: this explains the residual behaviour (third phase) at large

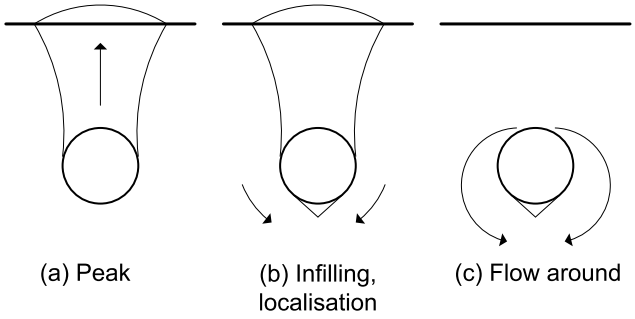

Figure 2: *Deformation mechanism observed during pipe uplift. (Based on Figure 11 in [8])*

displacements illustrated in Figure 1.

Considering the application of anchor plates and the pattern in Figure 1, it is clear that the primary interest is the peak pull-out force, when the loading attains a maximum [22]. This maximum force is frequently plotted as a function of the embedment ratio, H/D, where H is the burial depth and D is the diameter of the plate.

There are many experimental data in the literature to compare with the reverse hopper theory developed here. These data were compared with the reverse hopper theory by digitizing graphs from Ilamparuthi et al. [15], Murray and Geddes [22], Trautmann et al. [30], Schupp et al. [28], Matyas and Davis [20], and Dickin [12].

3 The reverse hopper theory

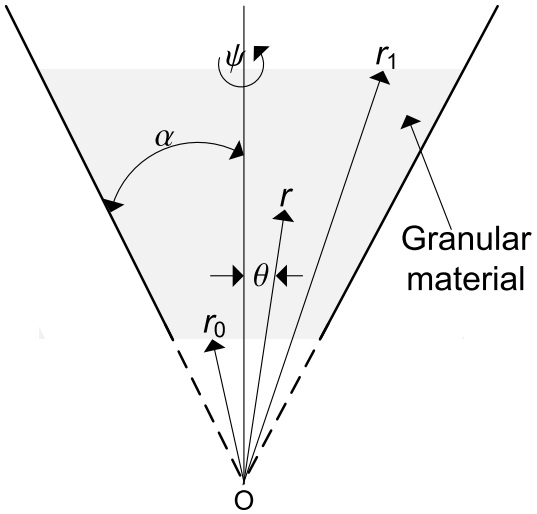

Figure 3: *Cross section of a hopper and the relevant dimensions used in the hopper theory.*

The theories for axi-symmetric and two-dimensional flow were developed from the hour-glass theory of Davidson and Nedderman [10]. The basic equations are not explained in detail, but are explained elsewhere [10]. The original hour-glass theory [10] predicted the flow-rate and stress distribution of granular materials in an ideal conical hopper. A similar theory was given by Nguyen et al. [24], Savage and Sayed [27] and Brennen and Pearce [7].

The objective of this theory is to predict the push up force against a surcharge of granular material above a buried object.

3.1 Axi-symmetric reverse hopper theory

In the original theory, the granular material flows downwards from a conical hopper, giving axi-symmetric flow. It is proposed that the push up of granular material in axi-symmetric flow can be approximated as a reverse hopper flow, leading to the development of the theory in this section. The theory assumes that the motion is radial, implying that the granules only move radially towards or away from point O in **Figure 3**. Hence, the granular material moves within a cone, the material outside the cone being stationary. A vertical section through the axis of the cone is illustrated in **Figure 4**.

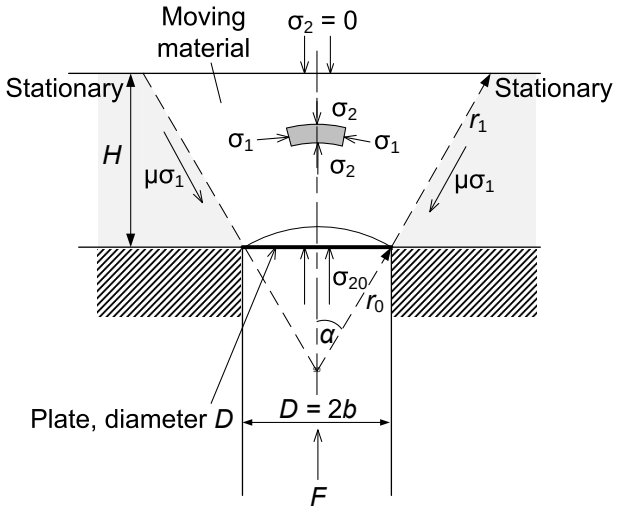

Figure 4: *Assumed upward flow of granular material when an upward force, F, is applied to the plate of diameter D. The grey areas highlight the stationary granular material.*

As reported by Davidson and Nedderman [10], the radial motion of the granular elements is described by

$$\rho v \frac{\mathrm{d}v}{\mathrm{d}r} = -\frac{1}{r^2}\frac{\partial}{\partial r}(r^2\sigma_\mathrm{r}) + \frac{\sigma_\theta + \sigma_\psi}{r} - \rho g \cos\theta, \tag{1}$$

where ρ is the bulk density of the granular material, v is the radial velocity, r is the radial distance, σ_r is the stress in the radial direction, σ_θ is the stress in the direction of θ, σ_ψ is the stress in the direction of ψ, and g is the acceleration of gravity. The directions of r, θ, and ψ are indicated in Figure 3.

Particle velocities are negligible, so the inertial term in Equation (1) can be ignored, giving

$$-\frac{1}{r^2}\frac{\mathrm{d}}{\mathrm{d}r}(r^2\sigma_r)+\frac{\sigma_\theta+\sigma_\psi}{r}-\rho g\,\cos\theta=0. \tag{2}$$

In the work reported below, it is assumed that θ is small, so $\cos\theta \simeq 1$. Assuming axial symmetry, $\sigma_\theta = \sigma_\psi$, as in hopper theory. Taking $\sigma_\theta = \sigma_\psi = \sigma_1$ and $\sigma_r = \sigma_2$, the stresses can be related through Equation (3). This is because the flow is active, with $\sigma_2 > \sigma_1$, where σ_2 is the major principal stress and σ_1 is the minor principal stress.

$$\sigma_2 = K\sigma_1, \tag{3}$$

where K is the coefficient of earth pressure, defined by

$$K = (1+\sin\phi)/(1-\sin\phi), \tag{4}$$

where ϕ is the angle of friction. It is a function of soil density, increasing with density [15]. Mohr's circle for the main body of the pushed up material is shown in **Figure 5**. Equation (3) is the important difference between the reverse hopper theory and the original hopper theory, for which the flow is passive and for which $\sigma_1 = K\sigma_2$.

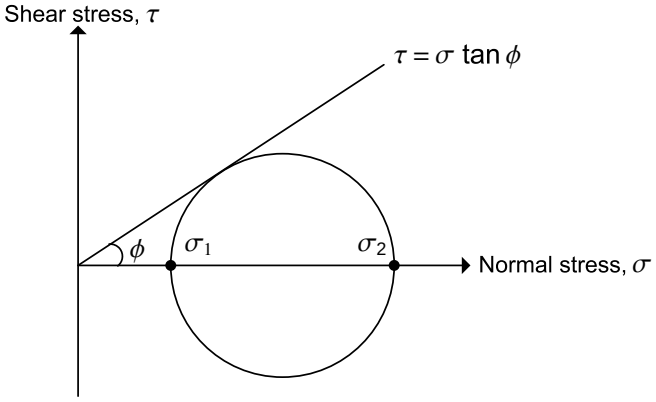

Figure 5: *Assumed Mohr's cirle for cohesionless granular material pushed up from below.*

The total push up force consists of two components. The first component, F_v, is due to the normal stresses σ_2, and the second component, F_s, is due to the shear stresses acting along the failure surface, assumed to be $\mu\sigma_1$ as shown in Figure 4.

3.1.1 Vertical component, from σ_2

The vertical stresses σ_2 arise from the weight of the granular material within the conical boundary shown in Figure 4.

The boundary condition is that $\sigma_2 = 0$ at the top surface where $r = r_1$, see Figure 4.

Applying Equation (3) and integrating Equation (2) with $\sigma_r = \sigma_2$, $\sigma_\theta = \sigma_\psi = \sigma_1 = \sigma_2/K$, $\cos\theta = 1$, and the boundary condition at $r = r_1$ gives

$$\sigma_2 r^{2\left(1-\frac{1}{K}\right)} = \frac{K\rho g}{3K-2}\left[r_1^{\left(3-\frac{2}{K}\right)} - r^{\left(3-\frac{2}{K}\right)}\right]. \tag{5}$$

When $r = r_0$, $\sigma_2 = \sigma_{20}$, giving, from Equation (5),

$$\sigma_{20} = \frac{K\rho g r_0}{3K-2}\left[\left(\frac{r_1}{r_0}\right)^{\left(3-\frac{2}{K}\right)} - 1\right]. \tag{6}$$

Davidson and Nedderman [10] proved that the velocity is insensitive to the angular position, indicated by θ in Figure 3. Therefore it can be assumed that σ_{20} does not change with θ.

The upward force F_v, due to σ_{20}, is calculated using Equations (6) and (7), by integrating along the curved surface of radius r_0, see Figure 4; $\cos\theta$ is included to resolve the force in the vertical direction, giving

$$F_v = \int_0^\alpha \sigma_{20}\, 2\pi\, r_0 \sin\theta\, r_0 \cos\theta\, \mathrm{d}\theta, \tag{7}$$

and hence

$$F_v = \sigma_{20}\,\left(\pi {r_0}^2/2\right)\left(1-\cos(2\alpha)\right). \tag{8}$$

Since $D = 2r_0\sin\alpha$, Equation (8) can be simplified to

$$F_v = \sigma_{20}\,\pi D^2/4. \tag{9}$$

3.1.2 Shear component, from σ_1

The normal stress σ_1 can be found by using Equations (3) and (5), giving

$$\sigma_1 = \frac{\rho g}{3K-2}\left[\frac{{r_1}^{\left(3-\frac{2}{K}\right)}}{r^{\left(2-\frac{2}{K}\right)}} - r\right]. \tag{10}$$

We now assume that there is shear stress τ at the conical interface between the moving and stationary material, see Figure 4. Using the internal friction coefficient, $\mu = \tan\phi$, the shear stress is assumed to be $\tau = \mu\sigma_1$; this is inconsistent with the assumption that σ_1 is a principal stress, which implies zero shear stress, see Figure 5. However, the actual

normal stress at the boundary between stationary and moving material, see Figure 4, may be quite close to σ_1, justifying the assumption that $\tau = \mu\sigma_1$. By integrating over the conical boundary shown in Figure 4, the contribution of shear stress to the upward force, F_s, to lift the bottom plate is

$$F_s = \int_{r_0}^{r_1} \mu\sigma_1 \, 2\pi r \sin\alpha \, \cos\alpha \, \mathrm{d}r. \tag{11}$$

For an ideal Coulomb material, μ at the slip plane is defined by $\mu = \tan\phi$ at the point of incipient yield [23]. However, Blau [5] showed that the friction opposing the onset of incipient motion is often higher than the friction opposing the continuance of motion once it has started. The coefficient for incipient motion is the static coefficient of friction; the coefficient for flowing sand is the kinetic coefficient of friction. In Section 4, it is shown that the value of μ for flowing sand has to be lower than $\tan\phi$ to obtain a reasonable fit of theory to experiment, especially for results with loose sand, suggesting that the kinetic coefficient is appropriate for flowing sand.

Combining Equations (10) and (11), and rearranging, gives

$$F_s = \frac{2\pi\mu\rho g \, \sin\alpha \, \cos\alpha}{3K-2} \left[{r_1}^3 \left(\frac{K}{2} - \frac{1}{3} \right) - \frac{K {r_1}^{\left(3-\frac{2}{K}\right)} {r_0}^{\frac{2}{K}}}{2} + \frac{{r_0}^3}{3} \right]. \tag{12}$$

Note that Equation (10) gives the principal stress, derived on the assumption that the conical boundary indicated in Figure 4 is frictionless. As mentioned above, the actual normal stress on the conical boundary may not be much different from σ_1, obtained from Equation (10).

3.1.3 Total force and breakout factor

The total push up force, F, is the sum of the vertical and shear components,

$$F = F_v + F_s. \tag{13}$$

The total force can be expressed as a dimensionless breakout factor,

$$N_{qf} = F/\gamma' A_p H, \tag{14}$$

where $A_p = \pi D^2/4$, D is the plate diameter (see Figure 4), and $\gamma' = \rho g$; in geotechnical engineering, N_{qf} is often referred to as the dimensionless peak pullout load at the point where the load attains a maximum [15].

Based on Figure 4, r_0 and r_1 can be expressed as

$$r_0 = D/2\sin\alpha, \tag{15}$$

$$r_1 = H/\cos\alpha + D/2\sin\alpha, \tag{16}$$

where α is the half angle of the conical boundary in Figure 4, D is the diameter of the plate, and H is the depth of surcharge. Combining Equations (6), (9), and (12 - 16) gives, after eliminating σ_{20}, r_0, r_1, F_v, F_s, and F,

$$N_{\mathrm{qf}} = \frac{DK}{2H\,(3K-2)\sin\alpha}\left[\left(1+\frac{2H\tan\alpha}{D}\right)^{(3-2/K)}-1\right] \tag{17}$$
$$+\frac{\mu D\cos\alpha}{2H(3K-2)\sin^2\alpha}\left[\left(K-\frac{2}{3}\right)\left(1+\frac{2H\tan\alpha}{D}\right)^{3}-K\left(1+\frac{2H\tan\alpha}{D}\right)^{(3-2/K)}+\frac{2}{3}\right].$$

3.2 Two-dimensional reverse hopper theory

In this case, Figure 4 shows a section through the two-dimensional granular flow pattern: the thickness normal to the diagram is large compared with the dimensions in Figure 4. It can be treated as hopper flow between two infinitely long plates inclined at $+\alpha$ and $-\alpha$ to the vertical.

Davidson and Nedderman [10] give the equation of motion for the two-dimensional case as

$$-\rho v\frac{\mathrm{d}v}{\mathrm{d}r} = \frac{1}{r}\frac{\mathrm{d}}{\mathrm{d}r}(r\sigma_{\mathrm{r}}) - \frac{\sigma_\theta}{r} + \rho g. \tag{18}$$

The two-dimensional reverse hopper theory predicts the uplift force of a long rectangular plate of breadth B and length L, where $L \gg B$. **Figure 6** shows the dimensions of such a plate buried in granular material.

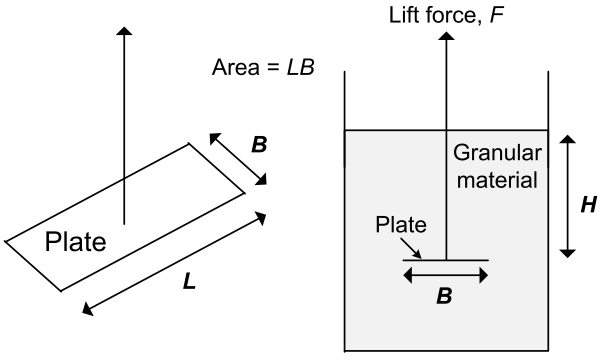

Figure 6: *Dimensions of a rectangular plate embedded in granular material; $L \gg B$.*

3.2.1 Vertical component, from $\sigma_{2\,(2D)}$

Since the flow is active,

$$\sigma_{2\,(2D)} = K\sigma_{1\,(2D)}, \tag{19}$$

where $\sigma_{1\,(2D)} = \sigma_\theta$ and $\sigma_{2\,(2D)} = \sigma_r$.

Combining Equations (18) and (19), and assuming negligible velocity v, gives

$$\frac{d\sigma_{2\,(2D)}}{dr} + \left(1 - \frac{1}{K}\right)\frac{\sigma_{2\,(2D)}}{r} + \rho g = 0. \tag{20}$$

Integrating Equation (20) and applying the top boundary condition as in the axi-symmetric case ($\sigma_{2\,(2D)} = 0$ at $r = r_1$) gives

$$\sigma_{2\,(2D)} = \frac{K\rho g r}{2K-1}\left[\left(\frac{r_1}{r}\right)^{\left(2-\frac{1}{K}\right)} - 1\right], \tag{21}$$

and

$$\sigma_{20\,(2D)} = \frac{K\rho g r_0}{2K-1}\left[\left(\frac{r_1}{r_0}\right)^{\left(2-\frac{1}{K}\right)} - 1\right], \tag{22}$$

where $\sigma_{20\,(2D)}$ is the value of $\sigma_{2\,(2D)}$ at $r = r_0$.

The upward force, $F_{v\,(2D)}$, contributed from $\sigma_{2\,(2D)}$, is calculated by integrating along the circular arc of radius r_0 in Figure 4,

$$F_{v\,(2D)} = \int_0^\alpha 2\sigma_{20\,(2D)}\, L\, r_0 \cos\theta \, d\theta, \tag{23}$$

which gives

$$F_{v\,(2D)} = 2\sigma_{20\,(2D)}\, L\, r_0 \sin\alpha, \tag{24}$$

where L is the distance in the direction normal to Figure 4.

3.2.2 Shear component, from $\sigma_{1\,(2D)}$

Combining Equations (19) and (21) gives the expression for the normal stress, $\sigma_{1\,(2D)}$, along the inclined planes,

$$\sigma_{1\,(2D)} = \frac{\rho g r}{2K-1}\left[\left(\frac{r_1}{r}\right)^{\left(2-\frac{1}{K}\right)} - 1\right]. \tag{25}$$

Assuming $\tau = \mu\sigma_{1\,(2D)}$, the frictional force, $F_{s\,(2D)}$, due to shear, is calculated by integrating along the inclined planes on both sides of the hopper,

$$F_{s\,(2D)} = \int_{r_0}^{r_1} 2L\mu\cos\alpha\ \sigma_{1\,(2D)} dr, \tag{26}$$

which gives, from Equations (25) and (26),

$$F_{s\,(2D)} = \frac{2L\rho g\mu\cos\alpha}{2K-1}\left[{r_1}^2\left(K - \frac{1}{2}\right) - K{r_1}^{\left(2-\frac{1}{K}\right)}{r_0}^{\left(\frac{1}{K}\right)} + \frac{{r_0}^2}{2}\right]. \tag{27}$$

3.2.3 Total force and breakout factor

The total push up force, F_{2D}, is the sum of the vertical and the shear components,

$$F_{2D} = F_{v\,(2D)} + F_{s\,(2D)}. \tag{28}$$

The breakout factor, $N_{qf\,(2D)}$, for the two-dimensional reverse hopper flow is defined by

$$N_{qf\,(2D)} = F_{2D}/\gamma' HBL. \tag{29}$$

Combining Equations (15) and (16), but with B in place of D, (22), (24), and (27 - 29) gives

$$N_{qf\,(2D)} = \frac{BK}{2H(2K-1)\sin\alpha}\left[\left(1+\frac{2H\tan\alpha}{B}\right)^{(2-1/K)} - 1\right] \tag{30}$$
$$+ \frac{\mu B\cos\alpha}{2H(2K-1)\sin^2\alpha}\left[\left(K-\frac{1}{2}\right)\left(1+\frac{2H\tan\alpha}{B}\right)^{2} - K\left(1+\frac{2H\tan\alpha}{B}\right)^{(2-1/K)} + \frac{1}{2}\right].$$

4 Results and discussion

In this section, the theory is compared with published experimental results. The main assumption in the comparison is that the theoretical force corresponds to the peak pullout load reported in the geotechnical engineering literature.

This section is divided into two parts. Section 4.1 compares axi-symmetric reverse hopper theory with uplift results on circular and rectangular plates. Section 4.2 compares two-dimensional reverse hopper theory with uplift results on rectangular plates and pipes.

The theory is dependent on the parameters ϕ, μ, and α, which are properties of the granular material. The value of ϕ is usually reported along with uplift data in the literature: **Table 1** lists recommended values for use in uplift models. However, the values of μ and α are very subjective, especially α which defines the failure surface. Cheuk et al. [8] measured the uplift mechanism using PIV (particle image velocimetry) and gives one of the best data sets on soil deformation during pipe/plate uplift. Nonetheless, there is insufficient information to approximate α as a function of soil properties and operating conditions.

Table 1: *Recommended values of ϕ [13].*

Sand type	$\phi(^\circ)$
Loose	30
Medium	35
Dense	40

4.1 Axi-symmetric reverse hopper theory in comparison with experimental data

4.1.1 Uplift of circular plates

This section presents experimental data on the uplift of circular plates obtained by Ilamparuthi et al. [15] who summarised uplift results from various papers. These data are compared with predictions from the reverse hopper theory.

Figure 7 presents the experimental data produced by Ilamparuthi et al. [15] and the theoretical curve from Equation (17). The points in Figure 7 are data obtained from uplift tests carried out with circular anchor plates of six different sizes (D = 100, 125, 150, 200, 300, and 400 mm) embedded at different depths in dense sand. Through direct shear tests, ϕ was measured at 43° for the sand. The theoretical line is plotted using Equation (17) with $\phi = 43°$, $\alpha = 35°$, and $\mu = \tan\ 43°$. The value used to approximate α is the average angle of inclination of the failure surface originating from the plate and measured by Ilamparuthi et al. [15] in failure mechanism tests for deep circular anchor plates. It is clear from Figure 7 that the agreement between the theoretical curve and the experimental data is excellent.

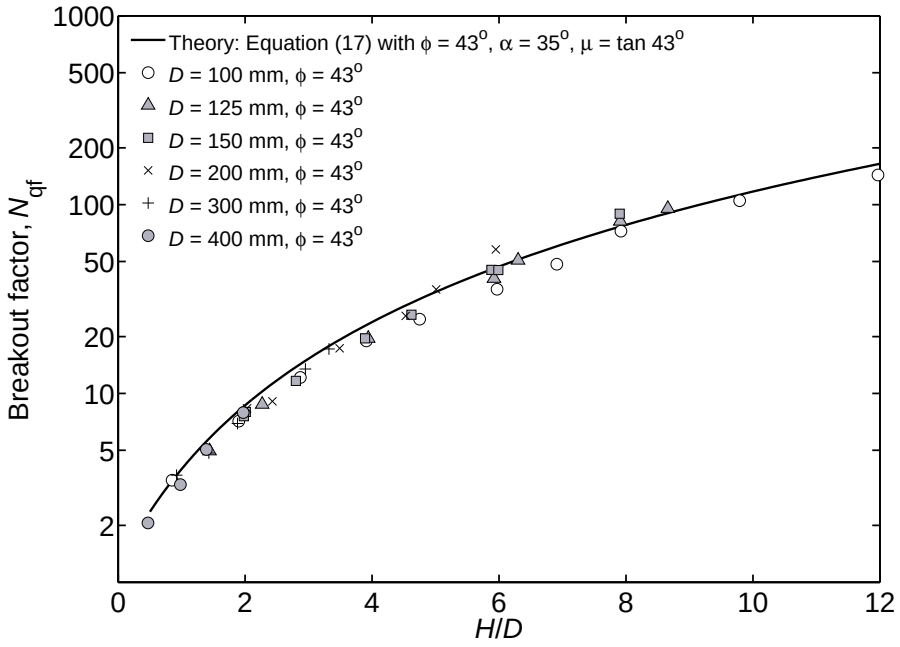

Figure 7: *Axi-symmetric reverse hopper theory, Equation (17), compared with the experimental data of Ilamparuthi et al. [Table 2, 15].*

Figure 8 presents the experimental results for circular plate anchors in medium-dense to dense sand from different sources. Two theoretical lines are plotted in Figure 8: one line is plotted using $\phi = 36^\circ$ (the lowest ϕ value within the data set), and the other line is plotted using $\phi = 46^\circ$ (the highest ϕ value within the data set). The principles used to choose the values of α and μ for the theoretical line in Figure 7 are applied in this case ($\mu = \tan\phi$ and $\alpha = 35^\circ$). Again, the agreement between the theoretical values and the experimental data is excellent, albeit overpredicting some of the experimental results, particularly results reported by Ilamparuthi et al. [15] from Andreadis and Harvey [1] for $\phi = 38^\circ$.

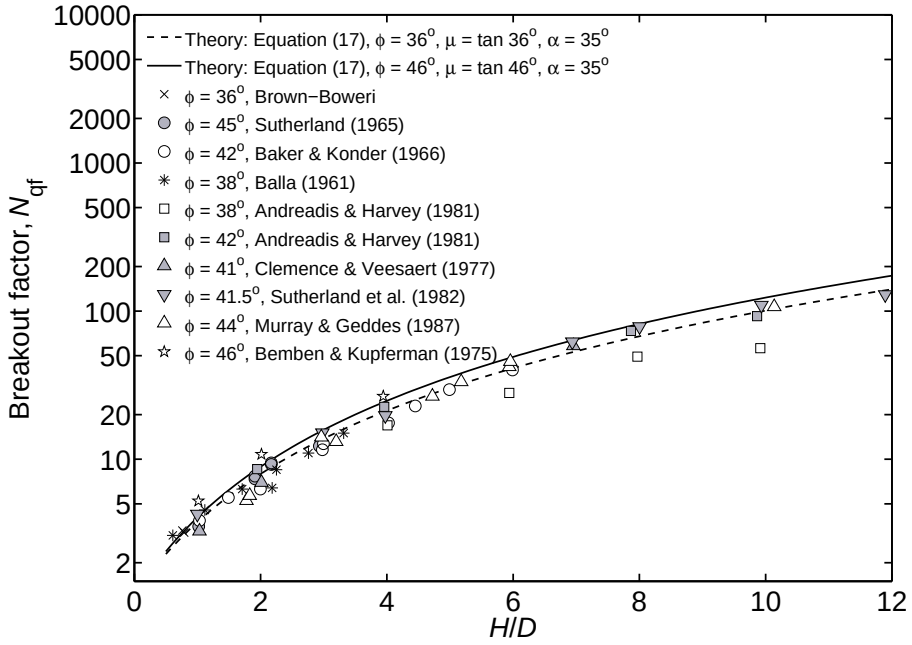

Figure 8: *Axi-symmetric reverse hopper theory, Equation (17), versus experimental data from uplift tests for circular plates in medium-dense to dense sand. (Experimental data compiled by Ilamparuthi et al. [Table 3 and Figure 16, 15].)*

Figure 9 presents the comparison between published experimental results for circular plate anchors in loose sand with the reverse hopper theory. It is evident from Figure 9 that using $\mu = \tan\phi$ gives theoretical lines which overpredict most of the data extracted from the literature, except the values from Kananyan [17]. It is found that lowering the value of μ to about $\tan(\phi/2)$ produces theoretical values which are closer to the data points. The need to lower μ is not observed for the results shown in Figures 7 and 8. This might be due to the fact that in the shear layer, at angle α to the vertical, the particles are looser than the bulk material due to motion, and hence $\mu < \tan\phi$.

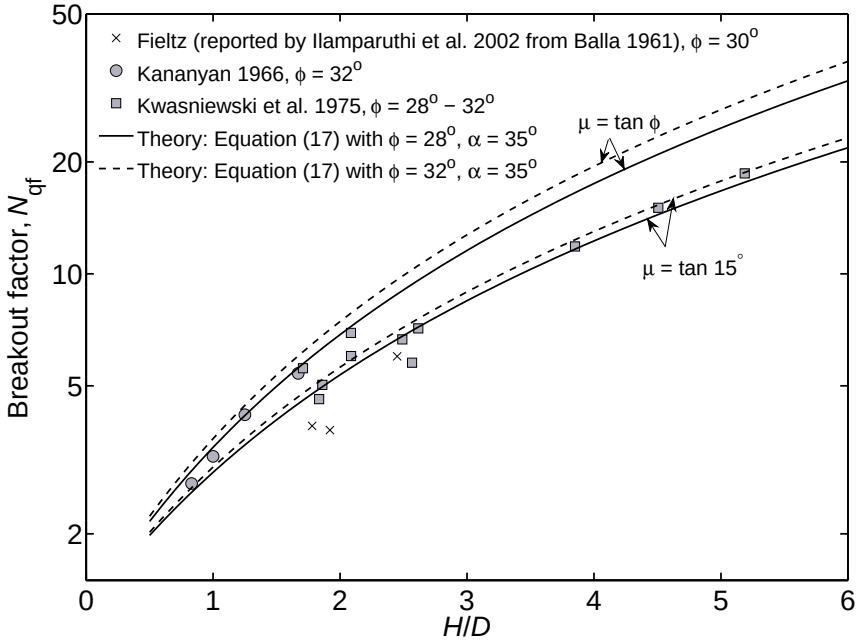

Figure 9: *Axi-symmetric reverse hopper theory, Equation (17), versus experimental data from uplift tests for circular plates in loose sand. Note that two values of μ are used to plot the theoretical lines. (Experimental data compiled by Ilamparuthi et al. [Table 3 and Figure 15, 15].)*

4.1.2 Uplift of rectangular plates

Equation (17) is suitable only for predicting the uplift force of circular plates because it describes force as a function of H/D, a dimensionless embedment ratio for circular plates. Rectangular plates have two relevant dimensions (length and breadth), so we define an equivalent embedment ratio,

$$H/D_e = H\sqrt{\pi/4LB}, \tag{31}$$

where $\pi {D_e}^2/4 = LB$ and D_e is the equivalent diameter of a circular plate giving the same area, LB, as the rectangular plate. Figure 6 shows the dimensions of a rectangular plate embedded in granular material.

Figures 10 and **11** present the uplift test results on rectangular plates reported by Murray and Geddes [22] and Dickin [12]: they performed uplift tests on rectangular plates with different length/breadth ratios ($L/B = 1, 2, 5, 8, 10$). The corresponding value of H/D_e, from Equation (31), for each rectangular plate data point was calculated to plot the data points in Figures 10 and 11.

Figure 10 presents the results for dense sand. Through direct shear tests, Murray and Geddes [22] reported that ϕ was measured at 44° for the sand used. However, Dickin [12] did not report a value of ϕ for the dense sand used, so the value $\phi = 44°$ is assumed

for both sets of data. The theoretical line is plotted using $\phi = 44°$, $\mu = \tan 44°$, and $\alpha = 32.5°$. The theoretical line is an almost perfect fit to the experimental data apart from the data of Dickin [12] for $H/D_e > 4$; this may be because the sand used by Dickin [12] had a lower value of ϕ.

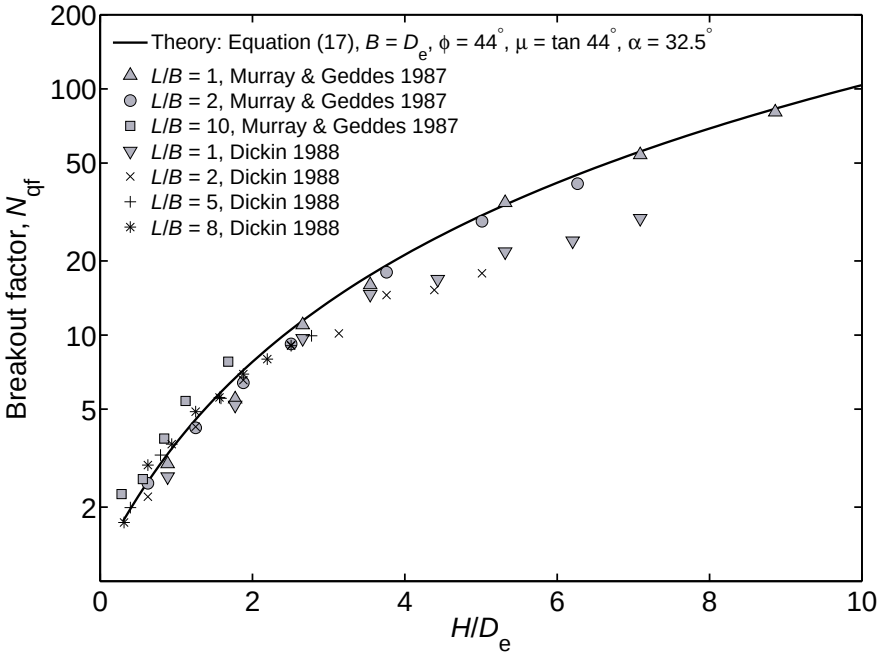

Figure 10: *Axi-symmetric reverse hopper theory, Equation (17), compared with experimental data from uplift tests for rectangular plates in dense sand. (Experimental data extracted from Murray and Geddes [Figure 3(a), 22] and [Figure 7, 12].)*

Figure 11 presents the results for loose sand. The ϕ value is not reported in the source of the data, so the value $\phi = 30°$ recommended by DNV [13] for loose sand was used to plot the theoretical line. In this case, the reverse hopper theory over predicts the breakout factor when $H/D_e > 4$. This may be caused by the fact that the axi-symmetric hopper theory is not suitable or the parameters ϕ, μ, and α are not appropriate for this data set.

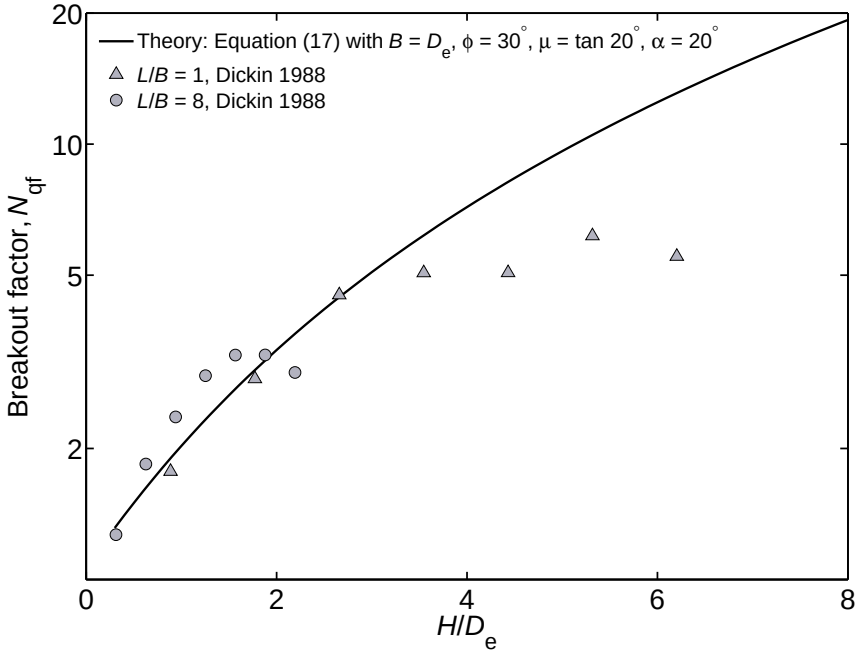

Figure 11: *Axi-symmetric reverse hopper theory, Equation (17), compared with experimental data from uplift tests for rectangular plates in loose sand. (Experimental data extracted from Dickin [Figure 7, 12].)*

4.2 Two-dimensional reverse hopper theory in comparison with experimental data

4.2.1 Uplift of pipes

Results from pipe uplift tests are used for comparison with the two-dimensional reverse hopper theory described in Section 3.2. These data are chosen because the uplift of pipes has been widely studied and the theory for lifting a rectangular plate is relevant to a pipe. The theoretical lines in this section are plotted using Equation (30).

When pipe uplift data are used, the pipe is assumed to be equivalent to a long plate and the pipe diameter, D_p, is taken as the plate anchor width, B. The shaded areas around the top part of the pipe illustrated in **Figure 12** are assumed to be rigid, mimicking the uplift of a rectangular plate. Nyman [25] proposed that the uplift of a buried pipe is analogous to that of a plate anchor, and the pipe diameter could be treated as the equivalent plate anchor width for deeply buried pipes. The results presented in **Figures 13** and **14** strengthen this claim because the theory predicts the dimensionless breakout factor reasonably well with plausible values of μ and α.

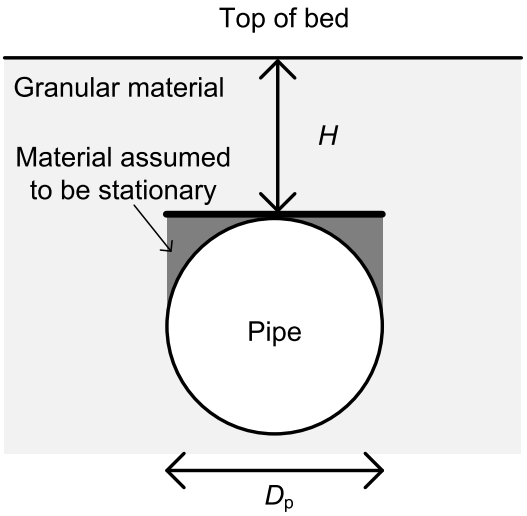

Figure 12: *Dimensions of a buried pipe. For comparison with theory, the pipe is treated as a long flat plate of width $B = D_p$, as indicated.*

Figure 13 presents pipe uplift test results on medium-dense to dense sand reported by Trautmann et al. [30] and Matyas and Davis [20]. The value of ϕ is not reported for these data. Hence, the value $\phi = 40^\circ$ recommended by DNV [13] for dense sand is used for the theory. By setting $\phi = 40^\circ$, $\mu = \tan 40^\circ$, and $\alpha = 20^\circ$, a theoretical line which compares well with the experimental data is obtained.

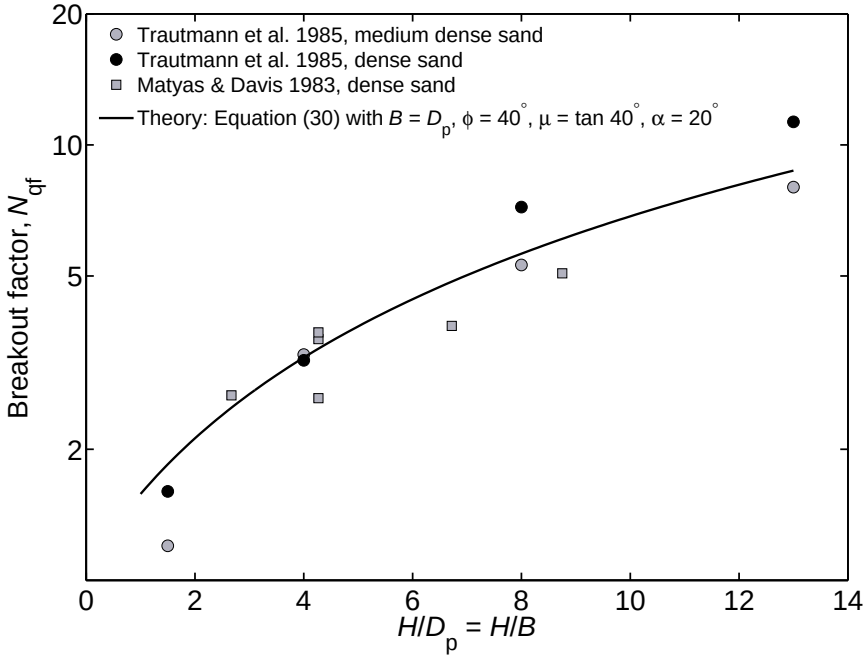

Figure 13: *Two-dimensional reverse hopper theory, Equation (30), compared with experimental data for pipe uplift tests in medium-dense to dense sand reported by Trautmann et al. [Table 2, 30] and Matyas and Davis [Table 2, 20].*

Figure 14 presents pipe uplift test results on loose sand reported by Trautmann et al. [30], Matyas and Davis [20] and Schupp et al. [28]. The value $\phi = 30^\circ$ recommended by DNV [13] for loose sand is used to plot the theoretical line. The theoretical line shown in Figure 14 is the best fit the authors could obtain by adjusting the values of μ and α. Both values of μ and α need to be lowered to obtain a reasonable fit. Lowering the value of μ below $\tan\phi$ is justified by the fact that the kinetic μ is usually lower than the static μ [5]. As for lowering the value of α, Ilamparuthi et al. [15] reported a lower α angle at low H/D_p from their measurements. However, there is insufficient information to draw a solid conclusion to determine the appropriate value of α for loose sands.

4.2.2 Uplift of rectangular plates

Figures 15, 16 and **17** present the experimental data shown in Figures 10 and 11, but plotted against H/B instead of H/D_e; the theoretical lines are plotted using Equation (30) instead of Equation (17). It is clear from Figures 15, 16 and 17 that the two-dimensional reverse hopper theory compares well with the data only at high L/B values and underpredicts the breakout factor at lower L/B values. Therefore, it can be concluded that the plate has to be long ($L/B \geq 8$) in order to ignore the end effects and apply the reverse two-dimensional hopper theory instead of the axi-symmetric theory.

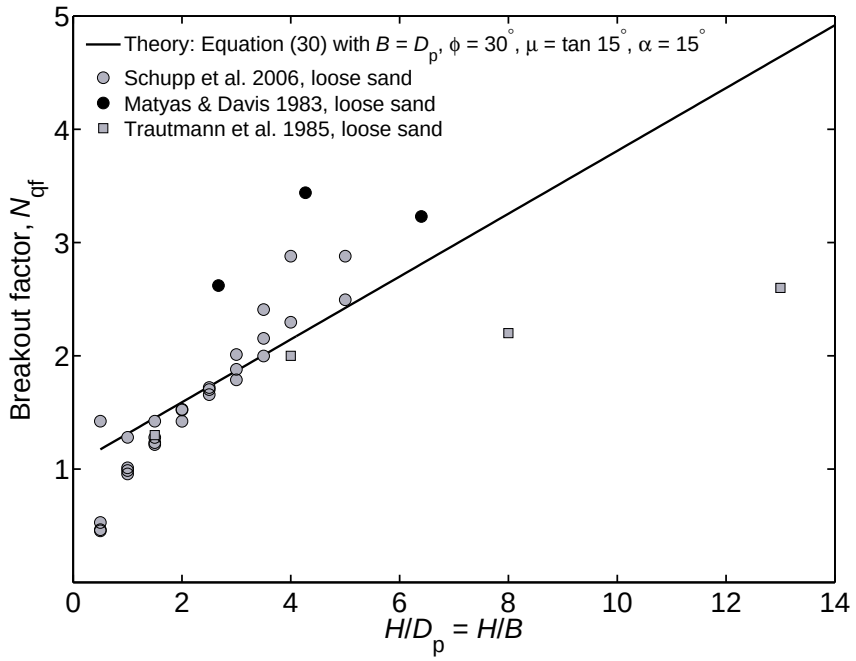

Figure 14: *Two-dimensional reverse hopper theory, Equation (30), compared with experimental data for pipe uplift tests in loose sand reported by Schupp et al. [Figure 7, 28], Matyas and Davis [Table 2, 20] and Trautmann et al. [Table 2, 30].*

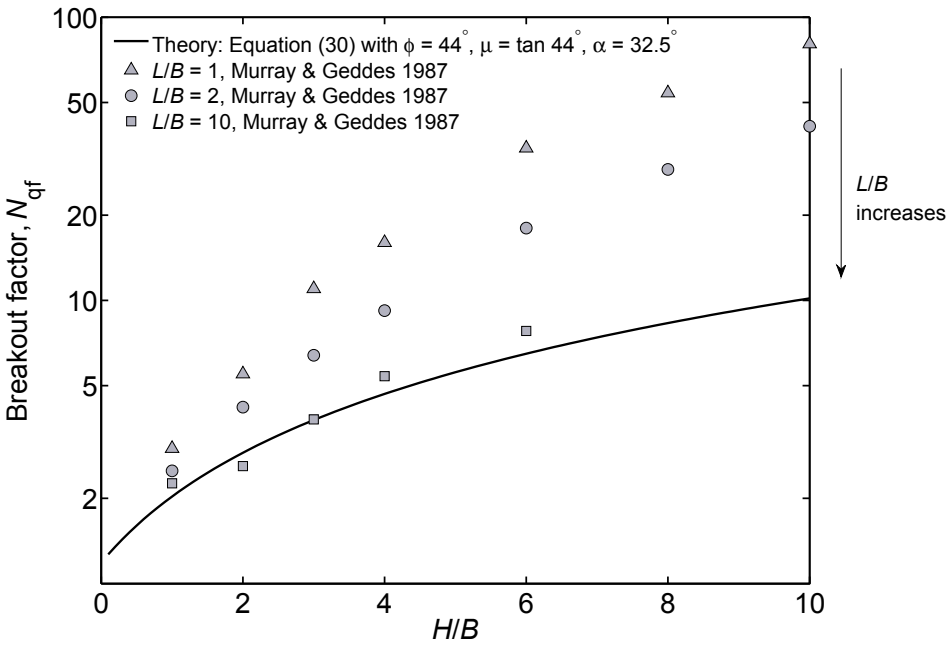

Figure 15: *Two-dimensional reverse hopper theory, Equation (30), compared with experimental data from uplift tests for rectangular plates in dense sand. (Experimental data extracted from Murray and Geddes [Figure 3(a), 22].)*

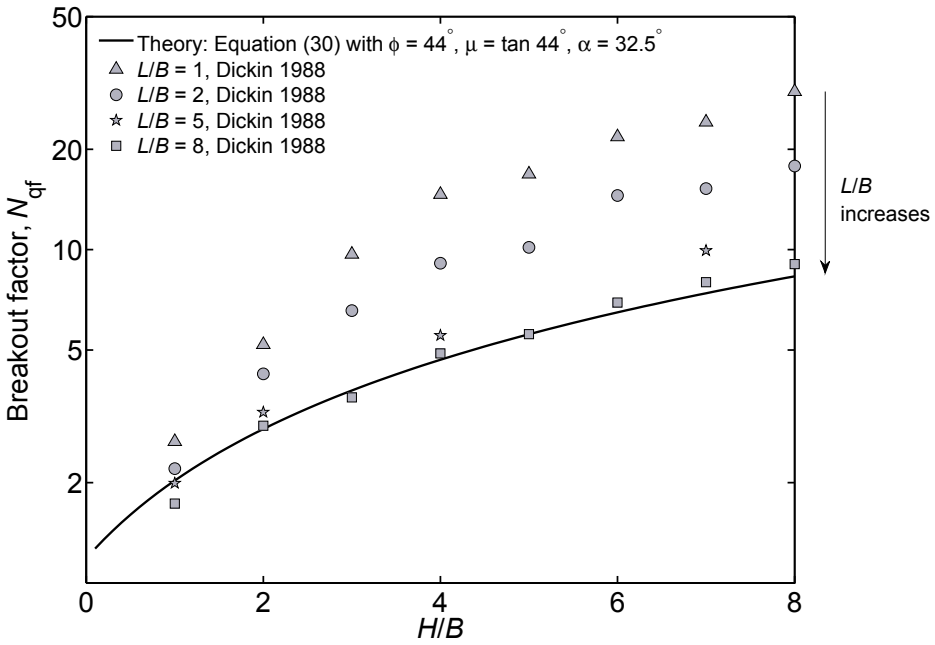

Figure 16: *Two-dimensional reverse hopper theory, Equation (30), compared with experimental data from uplift tests for rectangular plates in dense sand. (Experimental data extracted from Dickin [Figure 7, 12].)*

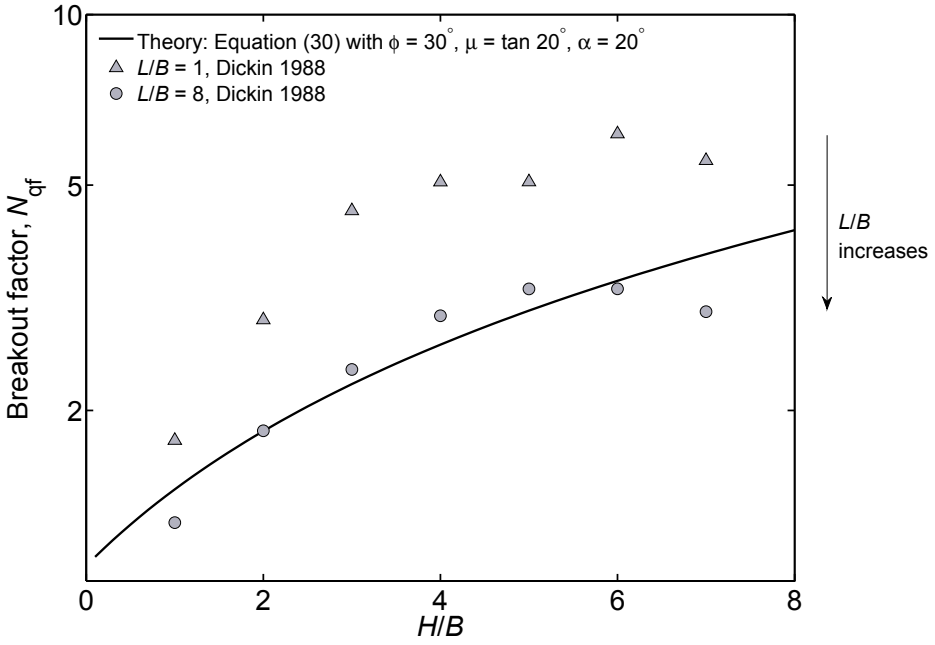

Figure 17: *Two-dimensional reverse hopper theory, Equation (30), compared with experimental data from uplift tests for rectangular plates in loose sand. (Experimental data extracted from Dickin [Figure 7, 12].)*

5 Conclusions

A new theory, developed in this work, improves the understanding of what happens during the start-up of a multi-nozzle fluidised bed. The main function of the theory is to predict the push up force required to unblock and mobilise the granular material above the nozzle.

The theory in this paper is developed from the hour-glass theory of hopper flow described by Davidson and Nedderman [10], but the particles are pushed up rather than flowing down. Two variations of the theory are presented. Both are derived using similar principles, but are suitable only for certain applications. The axi-symmetric reverse hopper theory is relevant to the fluidisation problem of particle movement above a nozzle and also for uplift of buried discs in granular material. The second variation, which is the two-dimensional reverse hopper theory, is appropriate for predicting the uplift of long pipes/plates embedded in granular material.

In this work, the theory has been extensively tested using published experimental data from geotechnical engineering. The results show that the new theory is able to predict most of the trends shown by the experimental data.

The existing uplift theories in geotechnical engineering were mostly derived by applying force balances around the assumed failure surface. Although not presented in this work, the reverse hopper theory is capable of predicting the effects of uplift rate because of the presence of the velocity term in Equations (1) and (18). This makes the reverse hopper theory unique compared to the existing uplift theories because this feature is not found in any of the existing theories. In this work, the velocity is assumed to be negligibly small because most of the uplift tests were done at a very slow rate.

The reverse hopper theory only solves the first half of the fluidisation problem investigated, which is to determine the minimum airflow to unblock a nozzle filled with particles. Hence, future work will focus towards extending the current model to include drag force on the particles due to airflow.

Acknowledgements

The authors are very grateful for continued support from Huntsman. The authors wish to thank the members of the Computational Modelling Group who have worked on this problem, particularly Richard Robinson, Gavin Williams and Sheryl Kuan. The authors are also grateful to Dr R M Nedderman for helpful discussions. MK acknowledges support by the Singapore National Research Foundation under its Campus for Research Excellence And Technological Enterprise (CREATE) programme.

Nomenclature

Roman symbols

A_b	Area of bed	m^2
A_p	Area of plate	m^2
a	Total area of the nozzles	m^2
B	Breadth of rectangular plate	m
b	Radius of nozzle	m
D	Diameter of plate	m
D_e	Equivalent diameter for a rectangular plate	m
D_p	Diameter of pipe	m
F	Total push up force for axi-symmetric hopper theory	N
F_s	Shear force for axi-symmetric hopper theory	N
F_v	Vertical force for axi-symmetric hopper theory	N
F_2D	Total push up force for two-dimensional hopper theory	N
$F_\mathrm{s\,(2D)}$	Shear force for two-dimensional hopper theory	N
$F_\mathrm{v\,(2D)}$	Vertical force for two-dimensional hopper theory	N
g	Acceleration of gravity	$\mathrm{m\ s}^{-2}$
H	Height of surcharge	m
L	Length of rectangular plate	m
K	$= (1+\sin\phi)/(1-\sin\phi)$. Coefficient of earth pressure	[-]
N_qf	$= F/(\gamma' A_\mathrm{p} H)$. Breakout factor for axi-symmetric hopper theory	[-]
$N_\mathrm{qf\,(2D)}$	$= F_\mathrm{2D}/(\gamma' HBL)$. Breakout factor for two-dimensional hopper theory	[-]
r	Radius	m
r_0	Radius to bottom of hopper	m
r_1	Radius to top of hopper	m
U_mf	Minimum fluidisation velocity	$\mathrm{m\ s}^{-1}$
U_N	Nozzle gas velocity	$\mathrm{m\ s}^{-1}$
v	Radial velocity	$\mathrm{m\ s}^{-1}$

Greek symbols

α	Half angle of the cone or between 2D failure surfaces	$(^\circ)$
γ'	Unit weight of granular material	$\mathrm{N\ m}^{-3}$
θ	Angular position from the central axis	$(^\circ)$
μ	Coefficient of friction	[-]
ρ	Bulk density of granular material	$\mathrm{kg\ m}^{-3}$
σ_r	Stress in the radial direction	$\mathrm{N\ m}^{-2}$
σ_θ	Stress in the direction of θ	$\mathrm{N\ m}^{-2}$
σ_ψ	Stress in the direction of ψ	$\mathrm{N\ m}^{-2}$
σ_1	Minor principal stress for axi-symmetric hopper theory	$\mathrm{N\ m}^{-2}$
σ_2	Major principal stress for axi-symmetric hopper theory	$\mathrm{N\ m}^{-2}$

σ_{20}	Major principal stress at r_0 for axi-symmetric hopper theory	N m^{-2}
$\sigma_{1\ (2D)}$	Minor principal stress for two-dimensional hopper theory	N m^{-2}
$\sigma_{2\ (2D)}$	Major principal stress for two-dimensional hopper theory	N m^{-2}
$\sigma_{20\ (2D)}$	Major principal stress at r_0 for two-dimensional hopper theory	N m^{-2}
ϕ	Angle of friction	$(^\circ)$
ψ	Angular position around the central axis	$(^\circ)$

References

[1] A. Andreadis and R. C. Harvey. A design procedure for embedded anchors. *Applied Ocean Research*, 3(4):171–182, 1981. doi:10.1016/0141-1187(81)90060-2.

[2] W. H. Baker and R. L. Kondner. Pullout load capacity of circular earth anchor buried in sand. *National Academy of Sciences, Highway Research Board, Report 108*, pages 1–10, 1966.

[3] A. Balla. The resistance to breaking out of mushroom foundations for pylons. In *Proceedings of the 5th International Conference on Soil Mechanics and Foundation Engineering*, volume 1, pages 569–576, Paris, France, 1961.

[4] S. M. Bemben and M. Kupferman. The vertical holding capacity of marine anchor flukes subjected to static and cyclic loading. In *Proceedings of the 7th Offshore Technology Conference*, pages 363–374, Houston, Tex., OTC2185, 1975. doi:10.4043/2185-MS.

[5] P. J. Blau. The significance and use of the friction coefficient. *Tribology International*, 34(9):585–591, 2001. doi:10.1016/S0301-679X(01)00050-0.

[6] M. D. Bolton. The strength and dilatancy of sands. *Géotechnique*, 36(1):65–78, 1986. doi:10.1680/geot.1986.36.1.65.

[7] C. Brennen and J. C. Pearce. Granular material flow in two-dimensional hoppers. *Journal of Applied Mechanics*, 45(1):43–50, 1978. URL `http://authors.library.caltech.edu/59/`.

[8] C. Y. Cheuk, D. J. White, and M. D. Bolton. Uplift mechanisms of pipes buried in sand. *Journal of Geotechnical and Geoenvironmental Engineering*, 134(2):154–163, 2008. doi:10.1061/(ASCE)1090-0241(2008)134:2(154).

[9] S. P. Clemence and C. J. Veesaert. Dynamic pullout resistance of anchors in sand. In *Proceedings of the International Conference on Soil-Structure Interaction*, pages 389–397, Roorkee, India, 1977.

[10] J. F. Davidson and R. M. Nedderman. The hour-glass theory of hopper flow. *Chemical Engineering Research and Design*, 51a:29–35, 1973. URL `http://archive.icheme.org/cgi-bin/somsid.cgi?type=header&record=1253`.

[11] R. Di Felice. Hydrodynamics of liquid fluidisation. *Chemical Engineering Science*, 50(8):1213–1245, 1995. doi:10.1016/0009-2509(95)98838-6.

[12] E. A. Dickin. Uplift behavior of horizontal anchor plates in sand. *Journal of geotechnical engineering*, 114(11):1300–1317, 1988. doi:10.1061/(ASCE)0733-9410(1988)114:11(1300).

[13] DNV. *Recommended practice, DNV-RP-F110: Global buckling of submarine pipelines - Structural design due to high temperature/high pressure*, page 44. Det Norske Veritas, Baerum, Norway, 2007. URL http://exchange.dnv.com/publishing/codes/download.asp?url=2007-10/rp-f110.pdf.

[14] D. Geldart. Types of gas fluidization. *Powder Technology*, 7(5):285–292, 1973. doi:10.1016/0032-5910(73)80037-3.

[15] K. Ilamparuthi, E. A. Dickin, and K. Muthukrisnaiah. Experimental investigation of the uplift behaviour of circular plate anchors embedded in sand. *Canadian Geotechnical Journal*, 39(3):648–664, 2002. doi:10.1139/T02-005.

[16] J. Ireland and M. F. Bransby. Rate effects during pipeline upheaval buckling in sand. *Proceedings of the ICE - Geotechnical Engineering*, 162(5):247–256, 2009. doi:10.1680/geng.2009.162.5.247.

[17] A. S. Kananyan. Experimental investigation of the stability of base of anchor foundations. *Soil Mechanics and Foundation Engineering*, 3(6):387–392, 1966. doi:10.1007/BF01702954.

[18] J. Kwaniewski, I. Sulikowska, and A. Walter. Anchors with vertical tie rods. In *Proceedings of the 1st Baltic Conference, Soil Mechanics and Foundation Engineering*, pages 122–133, Gdańsk, Poland, 1975.

[19] E. L. Matyas and J. B. Davis. Prediction of vertical earth loads on rigid pipes. *Journal of Geotechnical Engineering*, 109(2):190–201, 1983a. doi:10.1061/(ASCE)0733-9410(1983)109:2(190).

[20] E. L. Matyas and J. B. Davis. Experimental study of earth loads on rigid pipes. *Journal of Geotechnical Engineering*, 109(2):202–209, 1983b. doi:10.1061/(ASCE)0733-9410(1983)109:2(202).

[21] R. S. Merifield and S. W. Sloan. The ultimate pullout capacity of anchors in frictional soils. *Canadian Geotechnical Journal*, 43(8):852–868, 2006. doi:10.1139/T06-052.

[22] E. J. Murray and J. D. Geddes. Uplift of anchor plates in sand. *Journal of Geotechnical Engineering*, 113(3):202–215, 1987. doi:10.1061/(ASCE)0733-9410(1987)113:3(202).

[23] R. M. Nedderman. *Statics and Kinematics of Granular Materials*, page 25. Cambridge University Press, 1992.

[24] T. V. Nguyen, C. Brennen, and R. H. Sabersky. Gravity flow of granular materials in conical hoppers. *Journal of Applied Mechanics*, 46(3):529–535, 1979. URL http://resolver.caltech.edu/CaltechAUTHORS:NGUjam79.

[25] K. J. Nyman. Soil response against oblique motion of pipes. *Journal of Transportation Engineering*, 110(2):190–202, 1984. doi:10.1061/(ASCE)0733-947X(1984)110:2(190).

[26] A. C. Palmer, D. J. White, A. J. Baumgard, M. D. Bolton, A. J. Barefoot, M. Finch, T. Powell, A. S. Faranski, and J. A. S. Baldry. Uplift resistance of buried submarine pipelines: comparison between centrifuge modelling and full-scale tests. *Géotechnique*, 53(10):877–883, 2003. doi:10.1680/geot.2003.53.10.877.

[27] S. B. Savage and M. Sayed. Gravity flow of coarse cohesionless granular materials in conical hoppers. *Zeitschrift für angewandte Mathematik und Physik ZAMP*, 32 (2):125–143, 1981. doi:10.1007/BF00946743.

[28] J. Schupp, B. Byrne, N. Eacott, C. Martin, J. Oliphant, A. Maconochie, and D. Cathie. Pipeline unburial behaviour in loose sand. In *Proceedings of OMAE'06, 25th International Conference on Offshore Mechanics and Arctic Engineering*, Hamburg, Germany, 2006. URL http://www-civil.eng.ox.ac.uk/people/bwb/papers/OMAE2006_92542.pdf.

[29] H. B. Sutherland. Model studies of shaft raising through cohesionless soils. In *Proceedings of the 6th International Conference on Soil Mechanics and Foundation Engineering*, volume 2, pages 410–413, Montréal, 1965. URL http://trid.trb.org/view.aspx?id=126984.

[30] C. H. Trautmann, T. O'Rourke, and F. Kulhawy. Uplift force-displacement response of buried pipe. *Journal of Geotechnical Engineering*, 111(9):1061–1076, 1985. doi:10.1061/(ASCE)0733-9410(1985)111:9(1061).

[31] D. J. White, C. Y. Cheuk, and M. D. Bolton. The uplift resistance of pipes and plate anchors buried in sand. *Géotechnique*, 58(10):771–779, 2008. doi:10.1680/geot.2008.3692.